

In Situ Atomic Force Microscopy Study of Microstructure Dependent Inhibitor Adsorption Mechanism on Carbon Steel

H. Wang, B. Brown, S. Nestic
Institute for Corrosion Multiphase Technology
Department of Chemical & Biomolecular Engineering, Ohio University
342 West State Street
Athens, OH 45701
USA

A. Pailleret
Sorbonne Université, CNRS, Laboratoire Interfaces et Systèmes Electrochimiques (LISE, UMR 8235)
4 place Jussieu, (case courrier 133)
Paris, 75005
France

ABSTRACT

Organic surfactant-type corrosion inhibitors are widely applied in the oil and gas industry considering their high efficiency at low ppm concentrations. The investigation of organic inhibitor adsorption and inhibition mechanisms on carbon steel has been limited by the difficulties with surface characterization techniques at a molecular level. Atomic force microscopy (AFM) can provide localized visual observation, and can also achieve characterization of mechanical properties of an inhibitor film, through friction and surface stiffness measurements in multiple operational modes. Reported research has systematically studied the frictional properties of self-assembled surfactant monolayers on mica using lateral force microscopy. However, there has been no such studies done on carbon steels. In the work reported herein, in situ AFM topography measurements in contact mode, in situ AFM friction imaging and in situ AFM phase imaging techniques have been applied to investigate the influence of different microstructures present in a ferritic-pearlitic carbon steel on inhibitor adsorption mechanisms as well as corrosion inhibition of CO₂ corrosion. AFM c friction images show a large friction contrast between inhibitor covered cementite structures and ferrite structures, while in the absence of inhibitor this friction contrast almost disappears, indicating the inhibitor adsorption induced this difference. AFM phase images indicate no preferential adsorption of inhibitor on cementite or ferrite structures. These results indicate that either the adhesion force of inhibitor molecules on the cementite structures could be much smaller than on ferrite structures, or the molecular orientations of inhibitor molecules adsorbed on the cementite and ferrite structures could be different. In either case, it is hypothesized that the carbide component of the steel microstructure directly influences inhibitor adsorption, which could decrease inhibitor efficiency in ferritic/pearlitic regions and areas where iron carbide is more prevalent.

Key words: corrosion inhibitors, quaternary ammonium, carbon steel, in-situ atomic force microscopy, CO₂ corrosion, molecular simulations

© 2022 Association for Materials Protection and Performance (AMPP). All rights reserved. No part of this publication may be reproduced, stored in a retrieval system, or transmitted, in any form or by any means (electronic, mechanical, photocopying, recording, or otherwise) without the prior written permission of AMPP.

Positions and opinions advanced in this work are those of the author(s) and not necessarily those of AMPP. Responsibility for the content of the work lies solely with the author(s).

INTRODUCTION

Corrosion resistant alloys (CRAs) are used for many pipeline and wellhead components associated with oil and gas production environments but may be considered too costly for longer crude oil and natural gas production lines. Mitigation of internal corrosion for these types of pipelines is normally carried out by batch treatment or continuous injection of corrosion inhibitors, especially the surfactant type of organic inhibitors, which are more economical than using a CRA.^{1,2}

Current research regarding corrosion inhibition of carbon steel by organic corrosion inhibitors mainly focused on studying the influence of inhibitor concentration, solution pH and temperature on inhibition efficiency by weight loss measurement and electrochemical studies, involving for example potentiodynamic polarization and electrochemical impedance spectroscopy.^{3,4} These studies were used to evaluate the inhibitor efficiency for a specific inhibitor under specific test conditions, but most neglected to address the mechanisms related to formation of an adsorbed layer on a metal surface or the nature/structure of this layer. Some publications have investigated the relationship between inhibitor structure and mitigation performance.⁵⁻⁹ However, a molecular level understanding of carbon steel/aqueous inhibitor solution interface properties was always impeded by the traditional electrochemical methods, which cannot obtain the localized adsorption properties of inhibitor layers.

Atomic force microscopy (AFM) has already been used to study the topography of a carbon steel surface in the presence of a corrosion inhibitor.^{7,10} However, AFM was mainly used as a supportive technique only to verify the presence of inhibitor on carbon steel by use of topography images and measures decrease of surface roughness variation after adding the inhibitor, while the surface properties of adsorbed inhibitor film that include hardness, friction, adhesion, and structural orientations, which are more related to mitigation efficiency under pipe flow, have not been adequately characterized. These topographic studies alone could not provide insight into the correlation between inhibitor structure and corrosion inhibition mechanisms. However, although the application of AFM for the corrosion inhibitor field is relatively immature, there have already been a few studies characterizing mechanical properties of surfactant systems at a molecular level by AFM. Liu et al presented a systematic study of frictional properties of self-assembled double chain quaternary ammonium surfactant monolayers using lateral force microscopy.¹¹ By measuring the friction force on bare mica and on a surfactant monolayer covered mica, they found the frictional forces were greatly diminished with the addition of surfactant and the adsorbed surfactant film was found to have a viscoelastic nature as indicated by an observed plateau in friction force curves created by increasing the tip sliding velocity. Similar friction force measurements have also been adopted by Li et al to develop a mechanistic model for surfactant molecular orientations which fit into an observed super low friction regime.¹²

In the present study, in situ AFM topography measurements in contact mode, in situ AFM friction imaging and in situ AFM tapping mode phase imaging techniques have been applied to investigate the influence of different microstructures present in a ferritic-pearlitic carbon steel on inhibitor adsorption mechanisms as well as corrosion inhibition of CO₂ corrosion.

EXPERIMENTAL PROCEDURE

Materials and Solutions

In order to obtain the required types and purity of corrosion inhibitors, model compounds are routinely synthesized and characterized within our laboratory. The specific model compound used in this work have a polar head group, dimethylbenzylammonium, and a tetradecyl (-C₁₄H₂₉) hydrophobic tail, as shown in **Figure 1**. The shortened name for this structure is BDA-C14, corresponding to tetradecylbenzyltrimethylammonium, used in the form of its bromide salt.

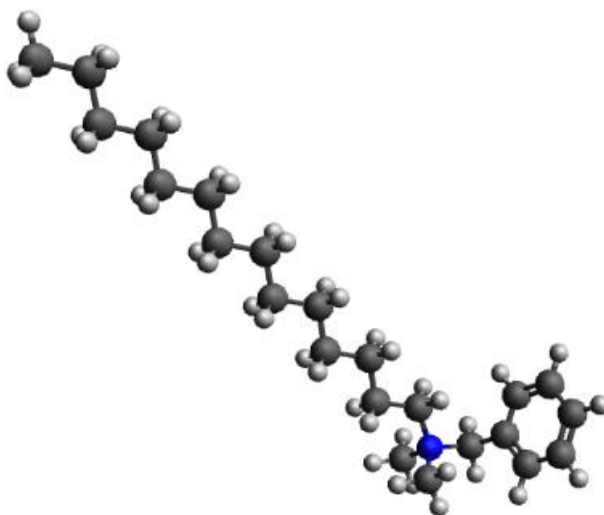


Figure 1. The molecular structure of tetradecylbenzyltrimethylammonium (BDA-C14)

Inhibitor concentration was selected based on its critical micelle concentration in a 1 wt.% NaCl electrolyte, specifically 100 ppm (2 CMC). The CMC of BDA-C14 was obtained by measuring changes in surface tension with concentration using the drop weight method.¹³ All solutions were prepared using deionized water with a conductivity of $18 \text{ M}\Omega \text{ cm}^{-1}$. The concentration of 2 CMC (100 ppm) was used in this work to obtain a full coverage film.

The steel specimen were machined from UNS G10180 carbon steel, and successively polished using 400, 600, 800, and 1200 grit silicon carbide abrasive papers followed by 9, 3, and $1 \mu\text{m}$ diamond particle loaded paste on a polishing cloth. The samples were then rinsed with acetone, ethanol and water and then dried in air.

In situ Contact Mode and Tapping Mode AFM Measurements

A commercial AFM (Molecular Imaging) was used to collect topography, friction, and phase images of the UNS G10180 steel surface in inhibitor solutions under an ambient CO_2 atmosphere by both contact mode and tapping mode consecutively in the same experiments. One V-shaped, silicon cantilever (HYDRA-ALL-G-50, AppNano) with standard normal spring constant of 0.049 N/m was used for both operation modes. The scan area was usually set as $10 \times 10 \mu\text{m}^2$ with the tip scanning at a speed of 8000 nm/s , and a resolution of 512 by 512 pixels was adopted for all AFM images.

During the contact mode AFM scanning, the cantilever bending (normal force) was kept at a constant value which is usually low enough to avoid removal of inhibitor film from the substrate surface. During operations both the height change and twisting of the cantilever were measured simultaneously and recorded as topography images and friction images, respectively.¹⁴

In order to avoid any lateral removal and shear effects at the tip-sample interface and retain the original adsorption morphology of the inhibitor film, tapping mode AFM was used.¹⁵ The phase image collected during tapping mode AFM operations records the phase lag of cantilever oscillation when the tip encounters a surface with different stiffness or hardness properties.^{16, 17} In this case, it was used for distinguishing soft inhibitor film and hard carbon steel substrate surfaces.

RESULTS

Comparison of Contact Mode AFM Topography and Friction Images- in the Presence of Inhibitor

Figure 2a and **2b** show $30 \times 30 \mu\text{m}$ AFM topography and friction images of the adsorbed film structures on the UNS G1018 steel surface in the presence of 1 wt.% NaCl solutions with BDA-C14 inhibitor model

© 2022 Association for Materials Protection and Performance (AMPP). All rights reserved. No part of this publication may be reproduced, stored in a retrieval system, or transmitted, in any form or by any means (electronic, mechanical, photocopying, recording, or otherwise) without the prior written permission of AMPP.

Positions and opinions advanced in this work are those of the author(s) and not necessarily those of AMPP. Responsibility for the content of the work lies solely with the author(s).

compound at 2 CMC. The topography image (**Figure 2a**) and friction image (**Figure 2b**) are obtained during the same line scan, but they show greatly different features. The surface topography resembles the originally polished surface in air, except for some features of slightly less deep polishing lines (the disappearance of the polishing lines over time is a sign of corrosion which occurred during the first few minutes of immersion before inhibitor adsorption. The fact that these lines did not appreciably change with time may be related to inhibitor adsorption. The friction image, however, shows several obvious lamellar structures in addition to the polishing lines seen in the topography image.

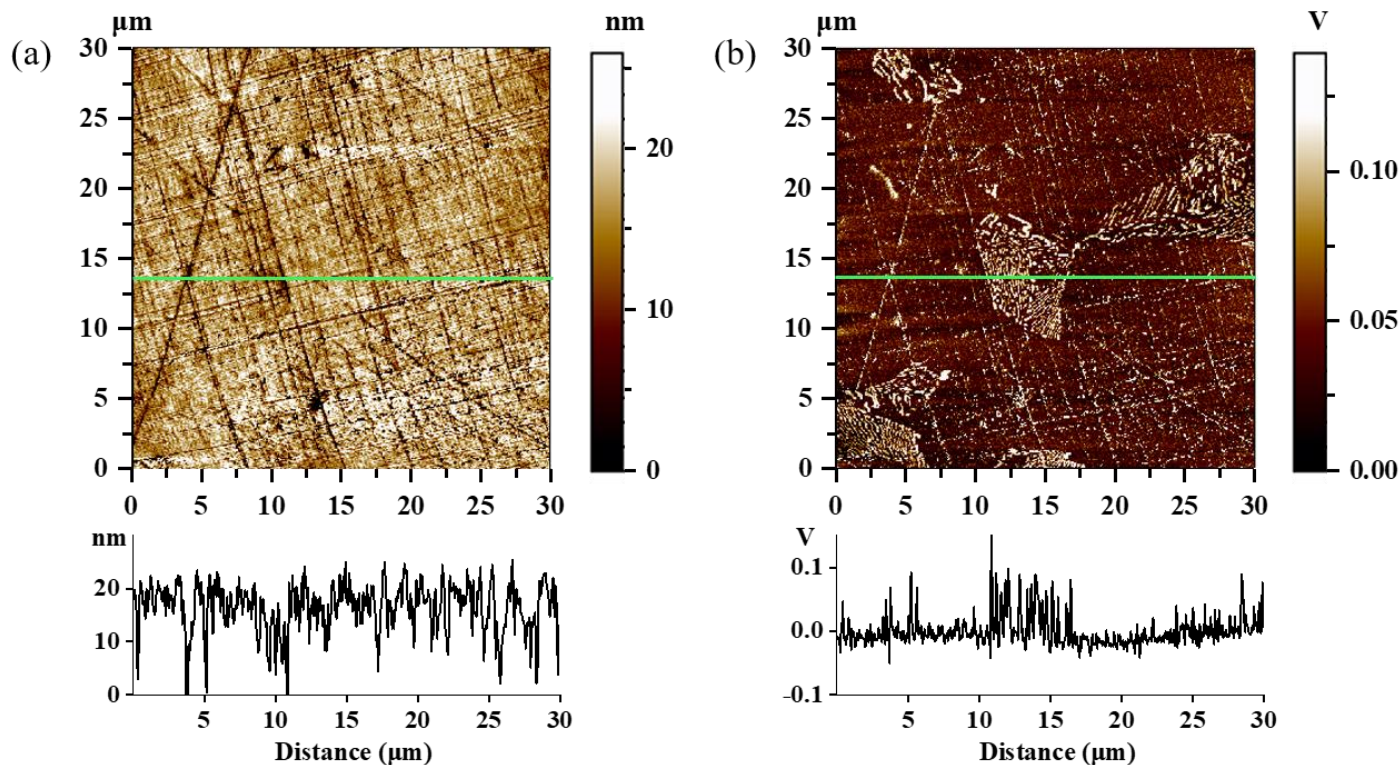


Figure 2. Contact mode AFM image of inhibitor film formed on UNS G1018 steel in a 2 CMC BDA-C14, 1 wt% NaCl solution: (a) topography image (b) friction image.

According to our previous studies related to the corrosion inhibition behavior of 1018 steel with the same inhibitor,¹⁸ these lamellar structures are cementite. The appearance of cementite can be caused by the ferrite preferentially corroding during the corrosion process. The 1018 steel is composed of a ferrite-pearlite microstructure, where pearlite consists of lamellar cementite structures filled with ferrite. As corrosion proceeds, the ferrite structure gradually dissolves while the cementite structure remains largely intact. A gradually increasing height difference between cementite and ferrite resulting from an expected corrosion phenomenon was detected by contact mode AFM topography images in our previous work.¹⁸ However, in **Figure 2b**, the cementite structures were only observed in friction images, while no such features emerged in topography images.

This situation has been repeatedly observed in multiple experiments **Figure 3a** and **3b** show two examples of small topographic contrast and large friction contrast obtained simultaneously on a same region of a 1018 steel sample in 2 CMC BDA-C14 inhibitor solution.

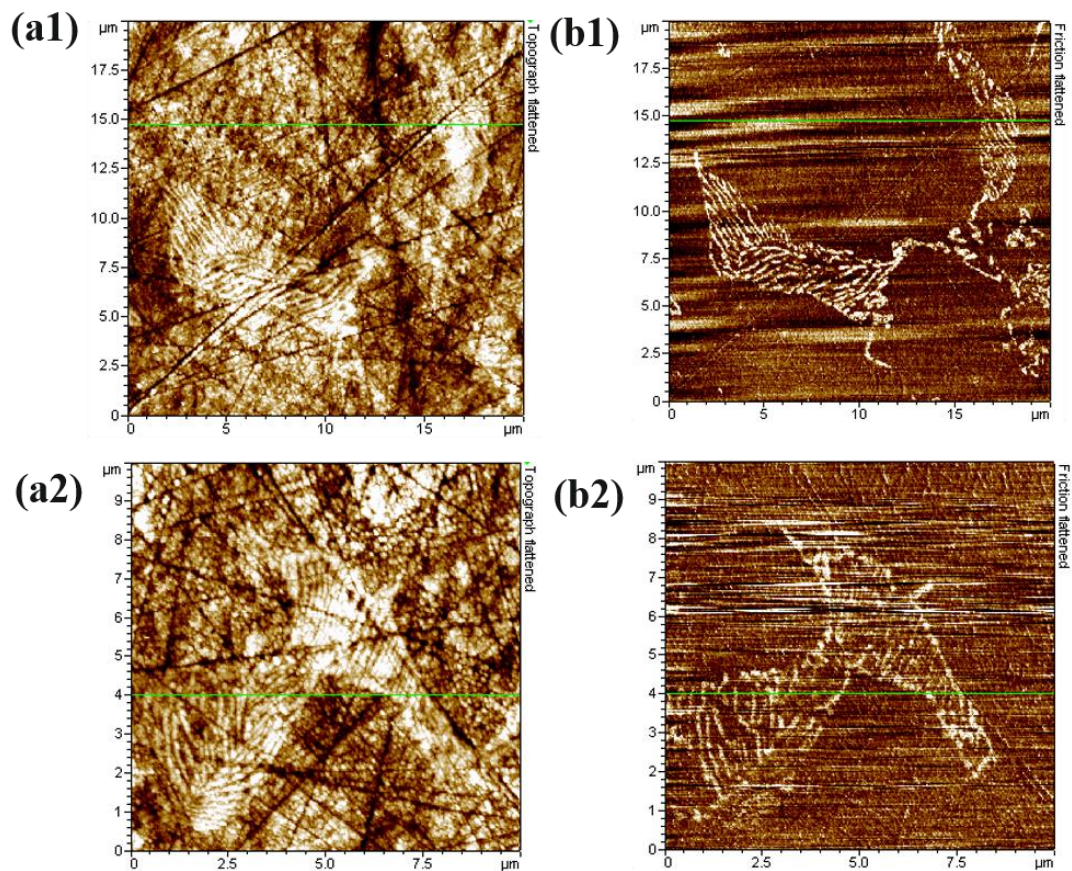


Figure 3. Contact mode AFM image of inhibitor film formed on UNS G10180 steel in a 2 CMC BDA-C14, 1 wt% NaCl solution: (a1) topography image-sample I (b1) friction image-sample I (a2) topography image-sample II (b2) friction image-sample II.

Figure 4 shows zoom in (scan size 10x10 μm) contact mode AFM images of the adsorbed film structures on 1018 steel surface in a 1 wt.% NaCl electrolyte with BDA-C14 inhibitor at 2 CMC. From this zoomed-in image, a clear friction contrast can still be seen (**Figure 4b**). The small height contrast related to cementite in the topography image (**Figure 4a**) indicates the corrosion was so slight that the height difference between cementite and ferrite is too small to be detected in the topographic image. As mentioned in the introduction, the friction contrast often includes topographic contributions. If the height contrast is large, the friction contrast would depend more on the height difference rather than pure friction difference. However, the small height contrast in **Figure 4a** implies that the friction force induced by height difference is reduced to a large extent or even can be neglected as the topographic contribution to friction contrast is almost negligible. Understanding of friction contrast phenomena is discussed in the following sections.

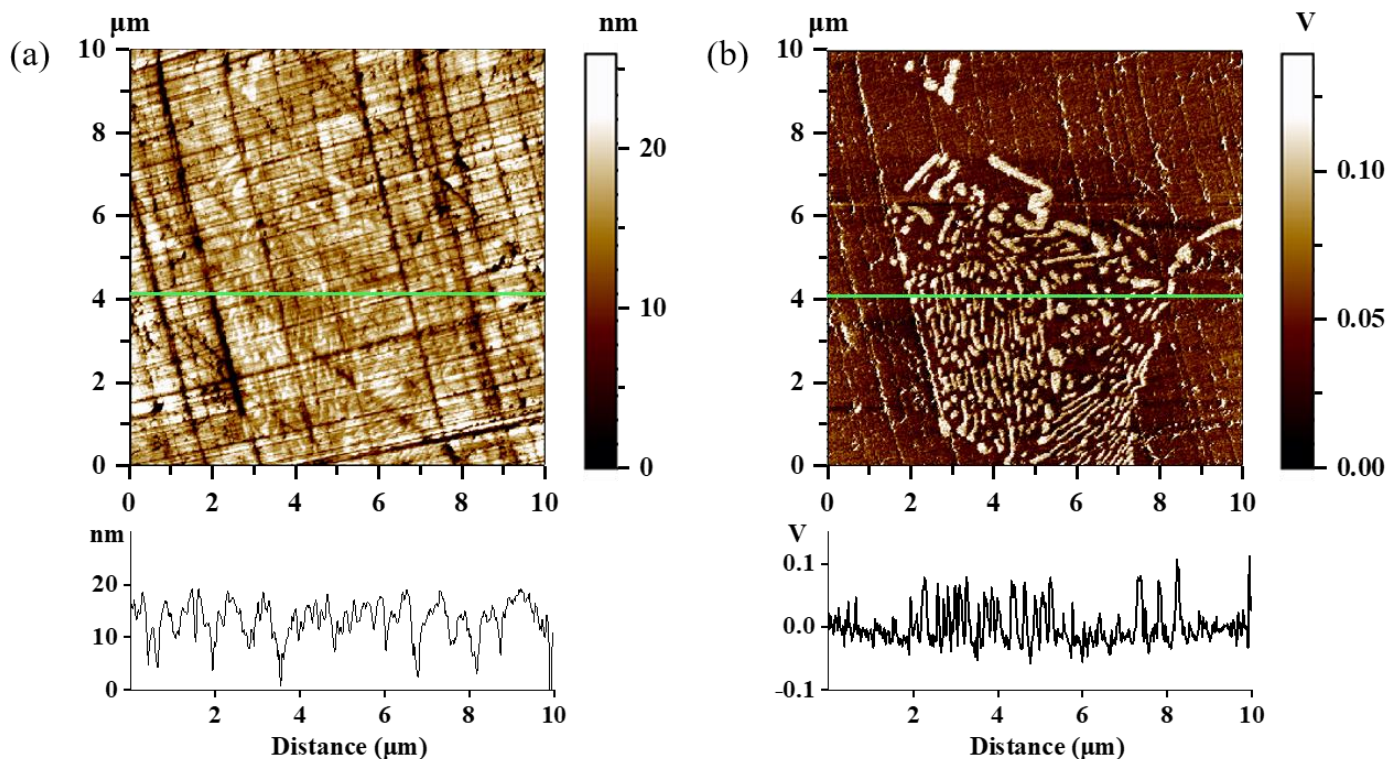


Figure 4. Contact mode AFM image of inhibitor film formed on UNS G1018 steel at 2 CMC BDA-C14, 1 wt% NaCl solution with scan size of 10 x 10 μm (zoom in): (a) topography image, (b) friction image.

The first question that needs to be addressed is whether the small change observed in the topography images is directly influencing the larger change observed in the friction images. **Figure 5** shows the cross-section profiles of three scan lines extracted from contact mode AFM images at specific locations, all measured from left to right, across the adsorbed film structures on the mild steel surface in 1wt% NaCl solution with BDA-C14 inhibitor at 2 CMC. The friction image from **Figure 4b** is used to reference where the cross-section lines were taken (**Figure 5a**). The topography cross section profiles (in black) and the friction cross section profiles (in red) for the three different scan lines have been plotted together as shown in **Figure 5b, c, and d** to see if there is a correlation.

It can be observed that the peaks on friction profile line graphs do not overlap with corresponding topographic peaks, indicating the friction image does not contain topography induced artefacts. Notice that in the region between 3 μm to 6 μm in **Figure 5d**, each line shows a 0.075 to 0.10V response to the frictional changes across the pearlite region while changes in the topography are 10 nm or less. The friction contrast was not caused by the height difference or the twist of the tip on the edge of the cementite structure. Therefore, the large friction contrast in **Figure 3** and **Figure 3** must be purely because of the friction force difference between tip and sample. The friction force between tip and cementite is much larger than the friction force between tip and ferrite structure so that the friction contrast is very clear.

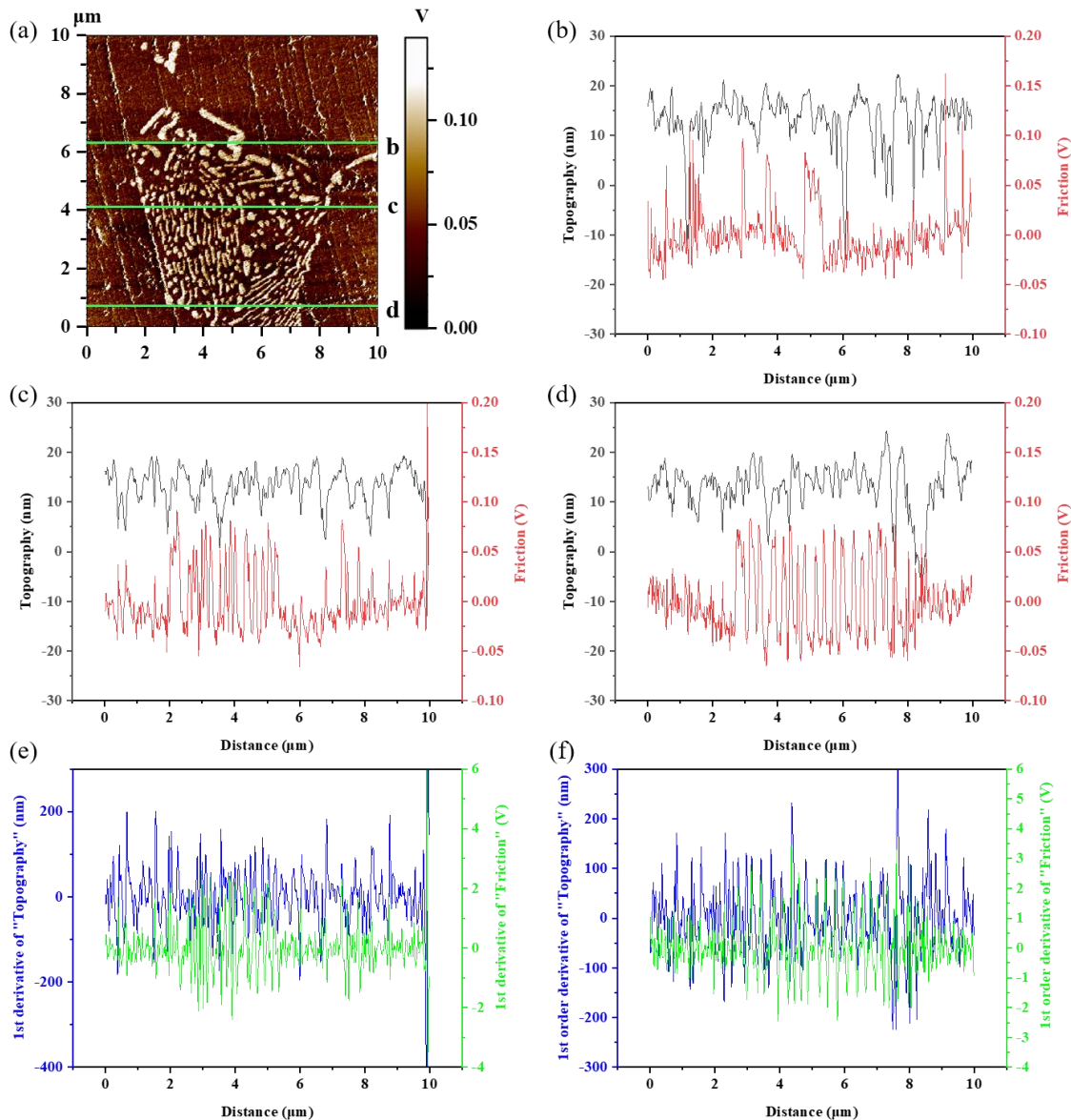


Figure 5. Cross section profile of topography and friction image-comparison: (a) friction image with cross section lines (b) line b (c) line c (d) line d (e) first order derivative of line c (f) first order derivative of line d

Figure 6 shows a further zoom-in (scan size 1 μm) image from the pearlite region of steel surface from the BDA-C14 inhibitor solution at 2 CMC concentration. Topography and friction data were collected by contact mode AFM imaging at the same time. However, the topography image is very different from the friction image. The large friction contrast between ferrite and cementite can still be observed from **Figure 6b**, and the topographic contrast is negligible (**Figure 6a**).

From the discussion above, this friction contrast means the AFM tip-to-covered cementite area friction force is larger than the AFM tip-to-covered ferrite area friction force. It is worth reminding that **Figure 6** was obtained in the presence of the inhibitor film, which means the tip is not directly in contact with the bare steel surface. Instead, the tip is directly scanning over the adsorbed inhibitor film surface which covers steel sample. Therefore, the friction contrast collected in the friction image was caused by the friction force between the AFM tip and the inhibitor film. There could be two possibilities which caused the friction difference: either the adsorbed inhibitor film surface had different mechanical properties, or

the underneath bare steel structures could have different mechanical properties which may induce a different friction force between tip and film.

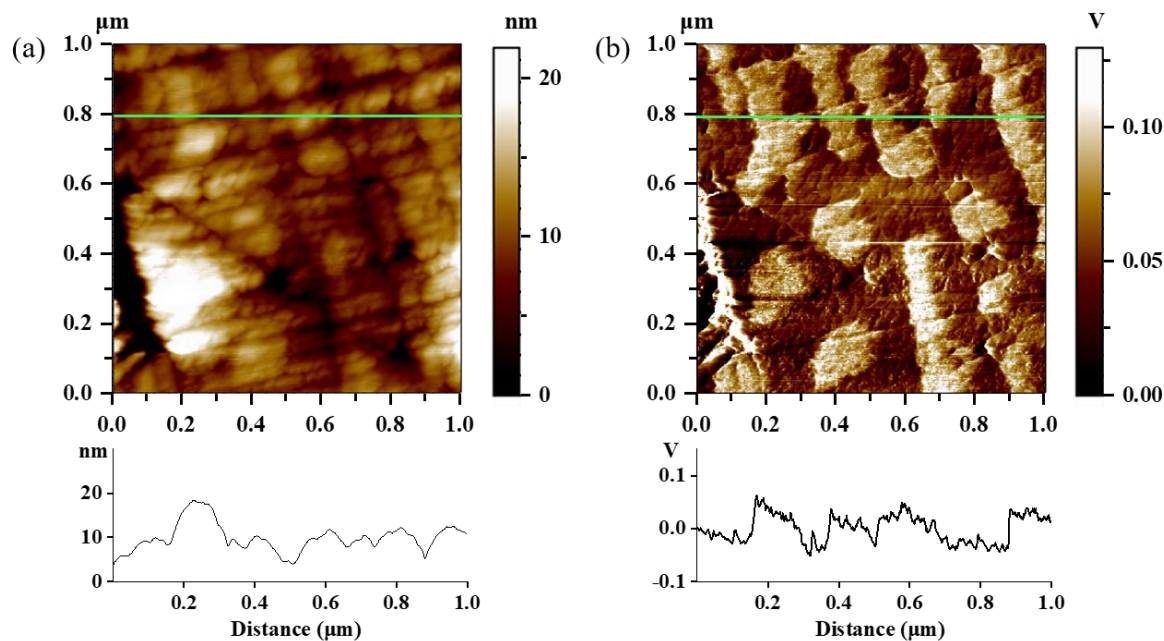


Figure 6. Contact mode AFM image of inhibitor film formed on UNS G1018 steel at 2 CMC BDA-C14, 1 wt% NaCl solution with scan size of 1 x 1 μm (further zoom in): (a) topography image, (b) friction image.

Comparison of Contact Mode AFM Topography and Friction Images- in the Absence of Inhibitor

In order to identify which possibility caused the friction contrast, the same contact mode AFM imaging was performed on 1018 steel in blank solution (no inhibitor), as shown in **Figure 7**. As can be seen from the topography image in blank solution (**Figure 7a**), the relatively high region (>300 nm in the line graph) is the cementite structure, whereas the lower region (100 – 200 nm) is the ferrite area. In the blank solution, the height contrast in the topography image is pretty large because corrosion proceeds very fast in the absence of an inhibitor. As shown in the friction image (**Figure 7b**), the friction contrast between the cementite structure and the ferrite structure is very small. A curved feature with a large (bright) friction signal was observed at the edge of cementite area due to the sudden increase of height from ferrite to cementite. The friction of individual bare cementite and ferrite areas in blank solution are quite close. This means the bare steel structure, cementite and ferrite, show a negligible friction contrast under contact mode AFM tip scan. Therefore, it can be inferred that the large friction contrast in **Figure 6** was induced by the adsorption of the inhibitor.

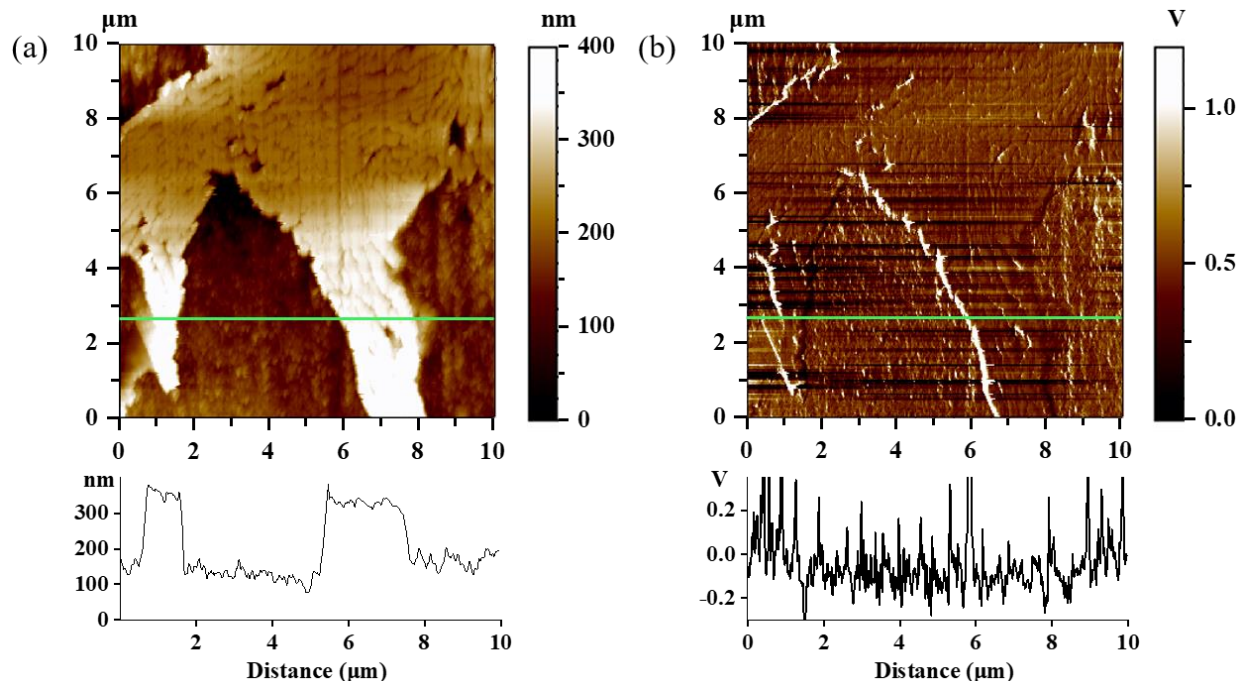


Figure 7. Contact mode AFM image of inhibitor film formed on UNS G1018 steel in a 1 wt% NaCl solution: (a) topography image, (b) friction image

Figure 8 shows the zoomed-in (scan size: 3 μm) image from the pearlite region of the 1018 steel surface in blank solution. Compared with the zoom in image from the pearlite region in BDA-C14 inhibitor solution, the friction contrast in blank solution is quite small.

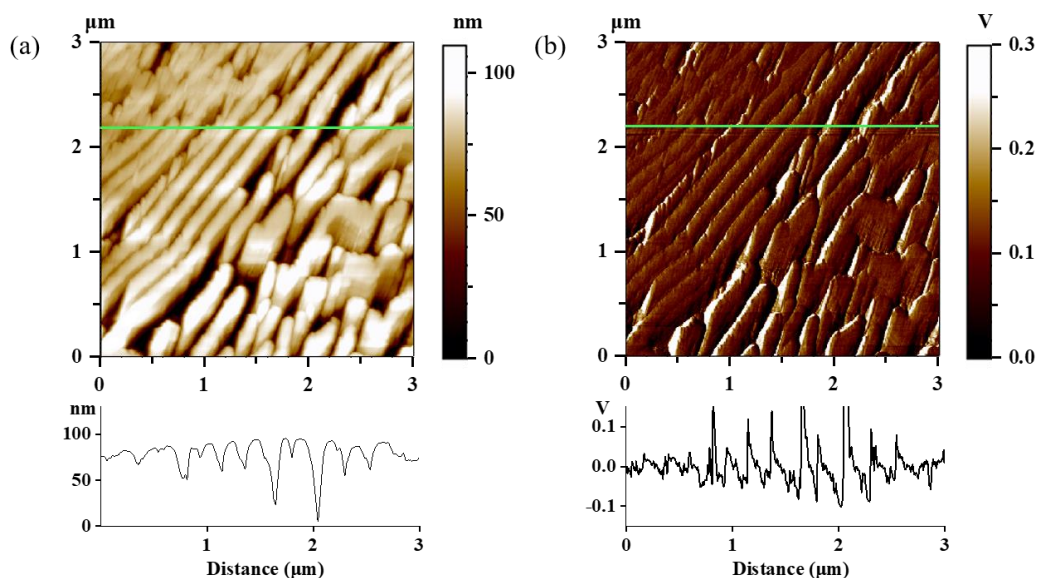


Figure 8. Contact mode AFM image of inhibitor film formed on UNS G1018 steel at 1 wt% NaCl solution with 3 x 3 μm scan size of cementite region: (a) topography image, (b) friction image.

Figure 9 shows the zoom in (scan size: 3 μm) image from the ferrite region of the steel surface in blank solution. The friction contrast (**Figure 9b**) is still small. The topography (**Figure 9a**) of ferrite showed spherical features after the polishing lines all dissolved during the corrosion process.

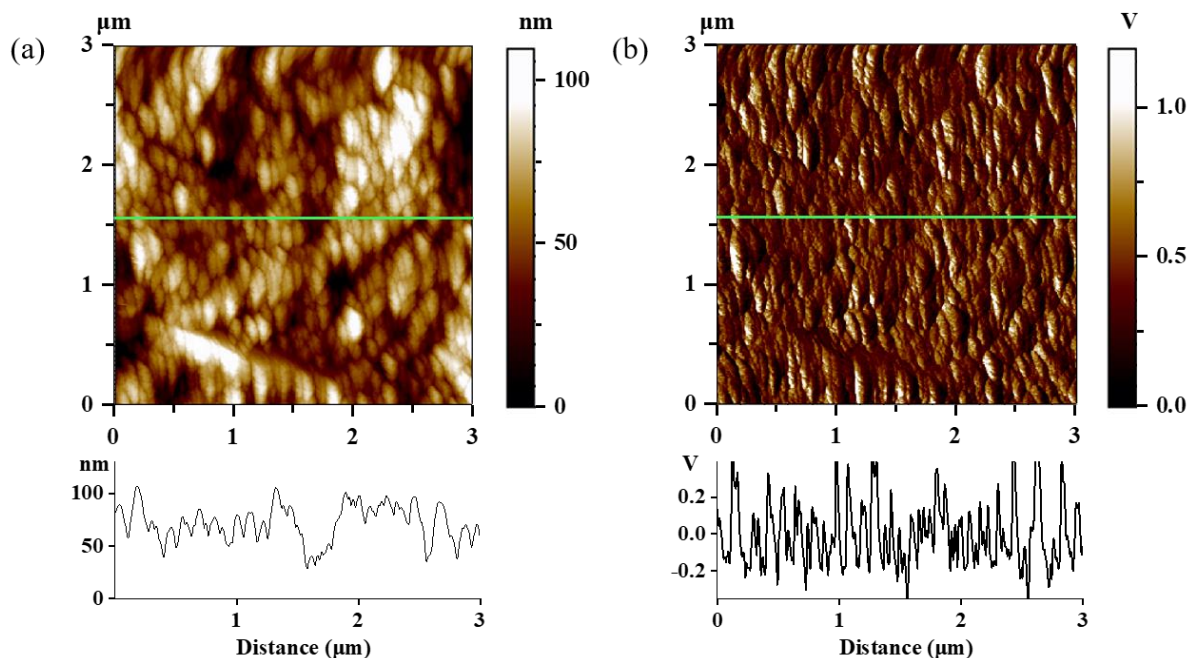


Figure 9. Contact mode AFM image of inhibitor film formed on UNS G1018 steel at 1 wt% NaCl solution with 3 x 3 μm scan size of ferrite region 3 μm scan size: (a) topography image, (b) friction image.

From the above discussion, it has been shown that the large friction contrast in **Figure 7b** and **Figure 9b** was induced by inhibitor adsorption. It can be assumed that there may be preferential adsorption of inhibitor on the ferrite structure, while the cementite structure could be void of any inhibitor. In this case, the friction contrast in **Figure 7b** would be due to the difference between the friction force on the inhibitor film covered surface and friction force on the bare steel structure surface. It is known from literature that the friction coefficient within a fluid (which is roughly like that within an inhibitor film) is much smaller than the friction coefficient for solid carbon steel, therefore the friction contrast between these two should be large. The friction coefficient is a dimensionless quantity whose magnitude indicates the relative ease of initiating or sustaining relative motion between two bodies that are being pressed together.¹⁹ In literature there is also much research related to the preferential adsorption mechanisms of molecular corrosion inhibitors on carbon steel samples, which seem to be happening here.^{8,9} However, further AFM evidence is needed to support or reject this preferential adsorption scenario.

Comparison of Contact Mode AFM and Tapping Mode AFM

In order to test the feasibility of the preferential adsorption scenario, tapping mode AFM imaging has been performed. The four images in **Figure 10** capture the exact same location on the 1018 steel surface in the 2 CMC BDA-C14 inhibitor solution using different AFM imaging modes. The defects with exactly the same shape in the four images identify the same location. The surface has been covered with inhibitor film in all four images. **Figure 10a1** and **b1** show the AFM topography and friction images obtained by using contact mode AFM. As discussed earlier, there is a large friction contrast (**Figure 10 b1**) and small topography contrast (**Figure 10 a1**) with contact mode AFM scanning. **Figure 10a2** and **b2** show AFM topography and phase images obtained by using tapping mode AFM. The phase image is used to map surface hardness. In a previous work, the phase image detected an exposed hard mica surface as a bright microdomain, while the soft inhibitor film was shown as black areas.²⁰ However, in the phase image in **Figure 10b2**, there is no clear phase contrast, and the cementite structure cannot be distinguished from just from the phase image. There is a rough outline of a lamellar cementite structure, but the phase contrast is very small. This indicates the hardness/softness measurement of the cementite and ferrite

surfaces in this inhibited solution are basically the same. This could lead to only one conclusion: both cementite and ferrite structures are covered with the inhibitor film, otherwise a larger friction contrast would be observed. Therefore, the phase image result (**Figure 10b2**) shows there was no preferential adsorption of inhibitor on different microstructures of 1018 steel. Inhibitor molecules covered the whole surface after initial adsorption.

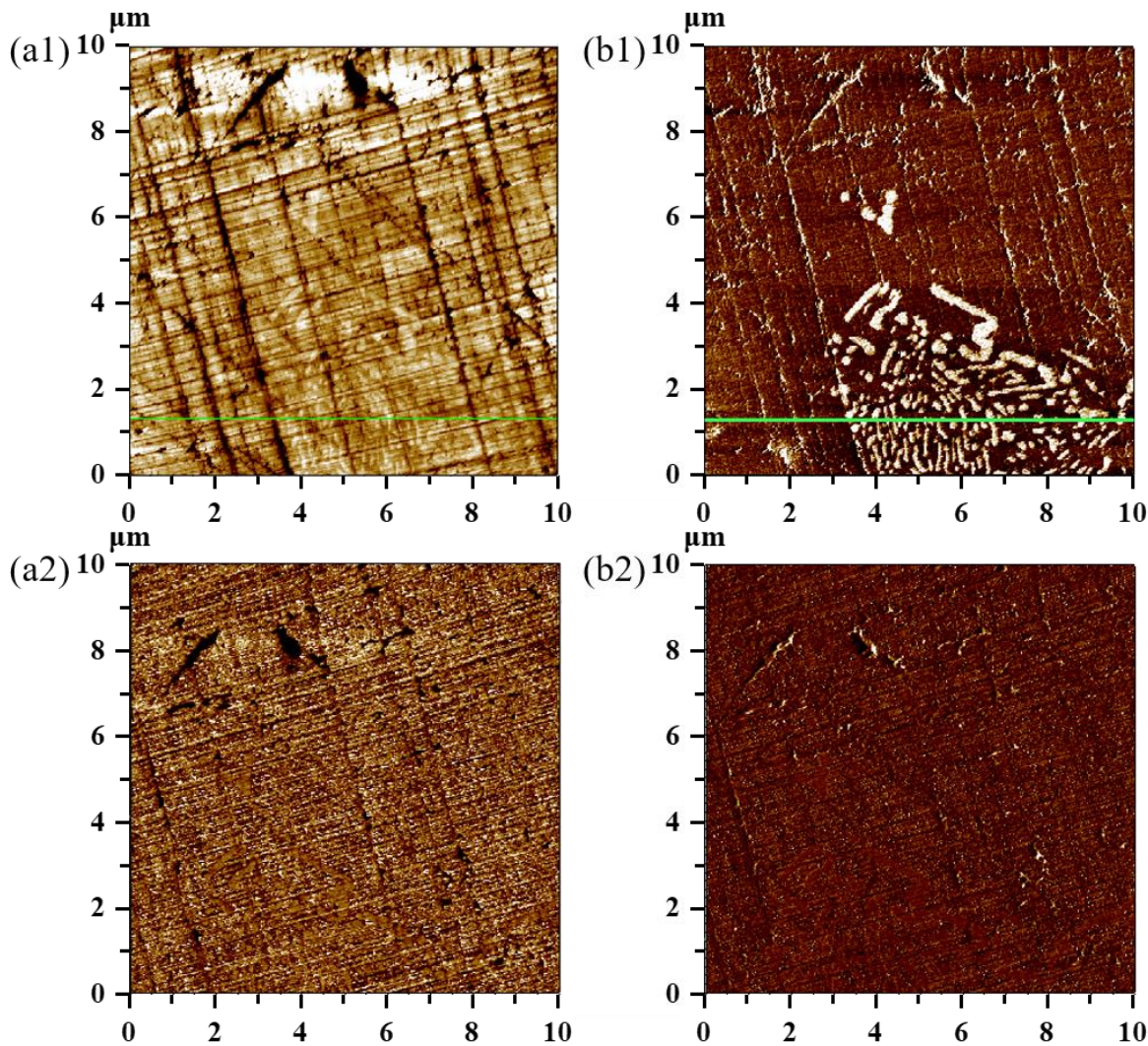


Figure 10. AFM image of inhibitor film formed on UNS G10180 steel in a 2 CMC BDA-C14, 1 wt% NaCl solution: (a1) topography image and (b1) friction image both obtained by using contact mode, (a2) topography image and (b2) phase image both obtained by using tapping mode.

Since the possibility of preferential adsorption has been disproven, it still needs to be resolved what caused the large friction contrast. The phase image result (**Figure 10b2**) shows that both cementite and ferrite structures have been uniformly covered with adsorbed inhibitor film after the initial adsorption, but the cementite region obviously showed a larger friction force with the AFM tip.

One explanation for the larger friction contrast during the contact mode scan is that the adhesion force of inhibitor molecules to cementite is smaller than the adhesion force of inhibitor molecules to ferrite. During a contact mode scan there is always a friction force between the tip and sample surface whose intensity depends on applied normal force. During a usual imaging scan (rather than scratching test), this friction force is kept at a small value because the applied normal force is expected to be 0, but it cannot be eliminated. It is possible that this small friction force is large enough to remove the inhibitor molecules from a cementite area, but may simultaneously not large enough to remove the inhibitor molecules from

a ferrite area. This difference would cause the indication of higher friction as the tip would contact the metal surface by removing the inhibitor film in the cementite area, but have lower friction in the ferrite area as the tip would slide over the softer, smoother inhibitor film surface without removing it.

For tapping mode, because the AFM tip intermittently taps on the steel surface during scanning, the lateral force can be neglected as it does not remove the inhibitor film from the cementite. Therefore, the phase imaging scan does not disturb the molecules adsorbed on the surface, which keeps the inhibitor film intact. The almost uniform softness displayed in the tapping mode phase image, **Figure 10b2**, indicates that both cementite and ferrite are covered with an inhibitor film.

To summarize this discussion, the tapping mode phase image (**Figure 10b2**) indicates there is no preferential adsorption of inhibitor and both cementite and ferrite microstructures are uniformly covered with the inhibitor film. However, the distinct contrast of areas in the contact mode friction image (**Figure 10b1**) indicates that the adhesion force of inhibitor molecules to cementite structures is much smaller than the adhesion force of inhibitor molecules to ferrite structures so that the inhibitor film on cementite structures is moved/removed easier by AFM tip friction forces.

This has raised concern that the inhibitor film on cementite microstructures could be easily removed by fluid flow. Previous AFM research from Xiong, et al., had calculated that the shear stress needed to remove an inhibitor film from X65 steel is larger than 60 MPa, which is at least four orders of magnitude higher than the wall shear stress generated by fluid flow.¹⁰ However, this measured high shear stress may be related more to the ferrite structure, while the shear stress needed to remove the inhibitor film from a cementite structure could be much lower. Further evaluation is needed to characterize friction forces and shear stress in order to verify this hypothesis.

Another possible explanation for the large friction contrast between cementite and ferrite is that there could be different molecular orientations for inhibitor molecules adsorbed on cementite and ferrite structures. The molecular orientations on the cementite structure could make the film less slippery.²¹

However, both explanations agree that it is possible for a corrosion inhibitor to have different adsorption behaviors on cementite and ferrite. This also agrees with previously published literature which observed that iron carbide can impair the corrosion inhibitor performance on carbon steels.^{9, 22} The difference in inhibitor adsorption behavior on ferrite and cementite microstructures could lead to more distinct separation of anodic and cathodic regions on an inhibited metal surface which may induce localized corrosion. More research is necessary in order to develop a better understanding of this phenomenon.

CONCLUSIONS

Based on contact mode and tapping mode AFM imaging results and proposed adsorption mechanism, these conclusions can be drawn:

- The BDA-C14 inhibitor showed no preferential adsorption on cementite vs. ferrite.
- The BDA-C14 inhibitor molecules seem to adsorb differently on cementite and ferrite; most likely there is be a different adhesion force or different molecular orientations on the two surfaces.
- This different adsorption of inhibitor molecules on cementite and ferrite could lead to a decrease in inhibitor efficiency and possibly to localized corrosion.

ACKNOWLEDGEMENTS

The authors would like to thank the following companies for their financial support: Ansys, Baker Hughes, BP America, Chevron Energy Technology, Clariant Corporation, CNOOC, ConocoPhillips, ExxonMobil, M-I SWACO (Schlumberger), Multi-Chem (Halliburton), Occidental Oil Company, Pertamina, Saudi Aramco, Shell Global Solutions, Sinclair Energy Partners, SINOPEC (China Petroleum), and TOTAL. Dr David Young is also thanked for synthesizing the BDA-C14 used in this work, as well as for assistance in preparing this paper.

REFERENCES

1. F. Bentiss, M. Lagrenee, M. Traisnel, J. Hornez, "The corrosion inhibition of mild steel in acidic media by a new triazole derivative, *Corrosion Science*, 41 (1999): pp. 789-803.
2. H. Luo, Y. Guan, K. Han, Inhibition of mild steel corrosion by sodium dodecyl benzene sulfonate and sodium oleate in acidic solutions, *Corrosion*, 54 (1998).
3. Y.J. Tan, S. Bailey, B. Kinsella, "An investigation of the formation and destruction of corrosion inhibitor films using electrochemical impedance spectroscopy (EIS)", *Corrosion Science*, 38 (1996): pp. 1545-1561.
4. C. Cao, "On electrochemical techniques for interface inhibitor research, *Corrosion Science*," 38 (1996): pp. 2073-2082.
5. J.D. Olivo, B. Brown, D. Young, S. Nešić, "Effect of Corrosion Inhibitor Alkyl Tail Length on the Electrochemical Process Governing CO₂ Corrosion of Mild Steel," *Corrosion*, 75 (2019): pp. 137-139.
6. I. Milošev, D. Zimerl, C. Carrière, S. Zanna, A. Seyeux, J. Iskra, S. Stavber, F. Chiter, M. Poberžnik, D. Costa, "Editors' choice—the effect of anchor group and alkyl backbone chain on performance of organic compounds as corrosion inhibitors for aluminum investigated using an integrative experimental-modeling approach, " *Journal of the Electrochemical Society*, 167 (2020): pp. 061509.
7. M. Yadav, S. Kumar, R. Sinha, I. Bahadur, E. Ebenso, "New pyrimidine derivatives as efficient organic inhibitors on mild steel corrosion in acidic medium: electrochemical, SEM, EDX, AFM and DFT studies, " *Journal of Molecular Liquids*, 211 (2015): pp. 135-145.
8. R. Zvauya, J. Dawson, "Inhibition studies in sweet corrosion systems by a quaternary ammonium compound," *Journal of Applied Electrochemistry*, 24 (1994): pp. 943-947.
9. S. Nestic, W. Wilhelmsen, S. Skjerve, and S. M. Hesjevik, "Testing of Inhibitors for CO₂ Corrosion Using the Electrochemical Techniques," (1995): pp. 1163-1192.
10. Y. Xiong, B. Brown, B. Kinsella, S. Nešić, A. Pailleret, "Atomic force microscopy study of the adsorption of surfactant corrosion inhibitor films," *Corrosion*, 70 (2014): pp. 247-260.
11. Y. Liu, D.F. Evans, Q. Song, D.W. Grainger, "Structure and frictional properties of self-assembled surfactant monolayers," *Langmuir*, 12 (1996): pp. 1235-1244.
12. J. Li, C. Zhang, P. Cheng, X. Chen, W. Wang, J. Luo, "AFM studies on liquid superlubricity between silica surfaces achieved with surfactant micelles, " *Langmuir*, 32 (2016): pp. 5593-5599.
13. B.-B. Lee, P. Ravindra, E.-S.J.C. Chan, S.A. Physicochemical, E. Aspects, "New drop weight analysis for surface tension determination of liquids," 332 (2009): pp. 112-120.
14. A.A. Baker, M.J. Miles, W. Helbert, "Internal structure of the starch granule revealed by AFM," *Carbohydrate research*, 330 (2001): pp. 249-256.
15. G. Xie, J. Ding, B. Zheng, W. Xue, "Investigation of adhesive and frictional behavior of GeSbTe films with AFM/FFM," *Tribology international*, 42 (2009): pp. 183-189.
16. P. James, M. Antognozzi, J. Tamayo, T. McMaster, J. Newton, M. Miles, "Interpretation of contrast in tapping mode AFM and shear force microscopy." A study of nafion, *Langmuir*, 17 (2001): pp. 349-360.
17. D. Polcari, P. Dauphin-Ducharme, J. Mauzeroll, "Scanning electrochemical microscopy: a comprehensive review of experimental parameters from 1989 to 2015," *Chemical reviews*, 116 (2016): pp. 13234-13278.
18. H. Wang, B. Brown, S. Nestic, A. Pailleret, "Investigation of Organic Inhibitor on Mild Steel using In Situ Atomic Force Microscopy and Electrochemical Measurement, " in: *NACE International Corrosion Conference Proceedings*, NACE International, 2020, pp. 1-14.
19. Britannica, "Coefficient of friction". The Editors of Encyclopaedia. *Encyclopedia Britannica*, 24 Jun. 2020, <https://www.britannica.com/science/coefficient-of-friction>. Accessed 2 July 2021.
20. H. Wang, B. Brown, A. Pailleret, S. Nestic, "Investigation of inhibitor adsorption mechanism by in situ tapping mode atomic force microscopy, " in: *NACE International Corrosion Conference Proceedings*, NACE International, 2021, pp. 1-14.
21. Li, J., Zhang, C., Cheng, P., Chen, X., Wang, W., and Luo, J. "AFM studies on liquid superlubricity between silica surfaces achieved with surfactant micelles," *Langmuir*, 32(2016): pp. 5593-5599.
22. A.A. Al-Asadi, *Iron Carbide Development and its Effect on Inhibitor Performance*, in, Ohio University, 2014.